

Empirical Validation of an Auxetic Structured Foot With the Powered Transfemoral Prosthesis

Woolim Hong , Namita Anil Kumar , Shawanee Patrick, Hui-Jin Um, Heon-Su Kim, Hak-Sung Kim , and Pilwon Hur 

I. INTRODUCTION

Abstract—The toe joint has been studied since it plays a critical role in human ambulation, such as stability, energy storage and propulsion. Despite its critical role, only a few studies have used and tested toe-jointed feet in powered prosthetic walking. In previous studies, we proposed 3D printable prosthetic feet with auxetic structures that provide human-like toe joint properties, termed a flat-toe (FT) foot and a curved-toe (CT) foot. The numerical simulation revealed that these feet could mimic the function of the biological toe joint, but they have not yet been validated in an empirical manner. In this study, we conducted a walking experiment with three subjects (i.e., two able-bodied and one amputee) using a powered prosthesis and two custom-designed prosthetic feet: the FT foot and CT foot. To evaluate the given feet, several metrics (e.g., joint kinematics/kinetics, ground reaction forces, and gait symmetry) were utilized. According to the results, the CT foot exhibited greater toe flexion, resulting in an earlier heel-off, a later toe-off, and a longer push-off duration when compared to the FT foot. Furthermore, less ground reaction forces were measured from both the prosthesis and intact sides, and a more symmetric gait was achieved with the CT foot. Another interesting finding was that the CT foot affected the user's thigh kinematics, leading to an improved gait phase estimation while walking. We concluded that the CT foot allowed for a more natural roll-over, resulting in better consistency and symmetry while walking with the powered prosthesis.

Index Terms—Auxetic structure, prosthetics and exoskeletons, prosthetic foot design, toe joint.

Manuscript received 7 February 2022; accepted 28 June 2022. Date of publication 28 July 2022; date of current version 29 August 2022. This letter was recommended for publication by Associate Editor A. Young and Editor J-H. Ryu upon evaluation of the reviewers' comments. This work was supported by the Korea Institute of Energy Technology Evaluation and Planning, the Ministry of Trade, Industry and Energy, Korean Government through Human Resources Development Program under Grant 20204010600090. (Corresponding author: Pilwon Hur.)

Woolim Hong and Namita Anil Kumar are with the Mechanical Engineering Department, Texas A&M University, College Station, TX 77843 USA (e-mail: ulim8819@tamu.edu; namita.anilkumar@tamu.edu).

Shawanee Patrick is with the College of Engineering, The Ohio State University, Columbus, OH 43210 USA (e-mail: spatrick2012@gmail.com).

Hui-Jin Um and Heon-Su Kim are with the Department of Mechanical Engineering, Hanyang University, Seoul 04763, South Korea (e-mail: gog9057@gmail.com; khsu0212@gmail.com).

Hak-Sung Kim is with the Faculty of the Department of Mechanical Engineering and the Institute of Nano Science and Technology, Hanyang University, Seoul 04763, South Korea (e-mail: kima@hanyang.ac.kr).

Pilwon Hur is with the Faculty of the School of Mechanical Engineering, Gwangju Institute of Science and Technology, Gwangju 61005, South Korea (e-mail: pilwonhur@gist.ac.kr).

This work involved human subjects or animals in its research. Approval of all ethical and experimental procedures and protocols was granted by the Institutional Review Board (IRB) at Texas A&M University (Application No. IRB2015-0607F).

Digital Object Identifier 10.1109/LRA.2022.3194673

THE toe joints are well known to play an important role in aiding stability [1] and energy storage and propulsion [2], [3] while walking. The toe joint stiffness also influences certain phases (e.g., push-off) of walking, altering joint kinematics and kinetics [4]–[6]. Furthermore, the curvature of the forefoot could improve foot rolling, influencing the mechanics and energetics of walking [7], [8]. Researchers at Vanderbilt University investigated the toe joint's functional effects on human walking by designing a passive toe joint mechanism using leaf springs to enhance their prosthesis performance [4]–[6]. Initially, they focused on the biomechanical effects of toe joint stiffness and toe shape by simply varying the given conditions [4]. As a result, as toe joint stiffness increased, so did push-off power [4]. The majority of participants (i.e., the healthy population), however, did not prefer the highest push-off condition. They rather preferred the condition of intermediate toe joint stiffness. This preference was investigated further with an amputee population using a custom-modified Balance Foot J (Ossur, Reykjavík, Iceland) [5]. Interestingly, the participants who had amputations on their dominant legs preferred the higher push-off condition, while the others preferred the intermediate level of push-off [5]. Moreover, the researchers investigated other parameters, such as toe length, foot arch (i.e., heel to toe joint) length, or toe joint axis, to quantify their effects on human walking biomechanics [6]. Changes in foot arch length had a greater impact on walking biomechanics (e.g., ankle push-off work) than changes in toe length, while changes in toe joint axis had little impact. By independently varying the given conditions (e.g., toe stiffness, toe length), the results of [4]–[6] provided several insights into the toe joint effect. However, they had less interest in how toe joint stiffness changes as the toe joint angle changes over the gait cycle. Some other studies have been conducted to benefit from the toe joint by mimicking its behavior for their prostheses [9]–[12]. Zhu et al. proposed a powered toe joint for their transtibial prosthesis [9]. They were able to replicate the nonlinear stiffness trend of the human toe joint, as shown in the angle-torque curve, by actively controlling the toe joint. Having an actuator at the toe, on the other hand, increased the weight of the system, possibly resulting in higher energy expenditure, hip work, and stress on the socket-residual limb connection [13]–[16]. Gabert et al. recently introduced a powered ankle/toe prosthesis with a five-bar mechanism for transtibial amputees [10]. In terms of weight, dimension, and build height, their design was comparable to the microprocessor-controlled prosthesis, and it was able to better

mimic the function of the human foot in a dynamic simulation. To be more exact, their foot used significantly less motor power and electrical energy than the foot without the toe joint [10].

We also attempted to mimic human toe joint kinematics and kinetics by applying the auxetic structures to a prosthetic foot design [11], [12]. The auxetic structure is known for its outstanding mechanical properties due to its negative Poisson's ratio, such as high energy absorption, shear and impact resistance [17], [18]. Thus, we implemented this structure in the prosthetic foot design to imitate a suitable deformation of the human toe joint in a stable manner while walking [11], [12]. Toe joint properties (e.g., toe flexion and nonlinear toe joint stiffness) were successfully mimicked with the auxetic structured foot in a simulation [11], [12], but its biomechanical effect has not yet been empirically validated when it is used with an actual prosthesis. Thus, the main objective of this study is to empirically validate the prosthetic feet proposed in the prior studies [11], [12] by conducting a walking experiment with two able-bodied subjects and one transfemoral amputee subject using the powered prosthesis. The contributions of this study are i) experimental validation of the 3D printed prosthetic feet that were created based on the auxetic structures, ii) joint kinematics and kinetics comparison between two prosthetic feet, and iii) gait symmetry comparison between two prosthetic feet. The remainder of this letter is structured as follows: Section II presents the preliminaries of this study. In this section, we briefly explain the prosthetic feet that we proposed in our previous works [11], [12]. Also, a custom-designed powered prosthesis and its control framework are described. Sections III and IV report the experimental protocols and results, respectively. We further discuss the results and the limitations of this study in Section V before concluding in Section VI.

II. PRELIMINARIES

A. Prosthetic Foot Design

We attempted to implement a flexible structure (i.e., auxetic) capable of mimicking human toe joint behavior while walking [11], [12]. We demonstrated that the auxetic structures could provide human toe joint properties (e.g., toe flexion and nonlinear toe joint stiffness), but the results were based solely on numerical simulation (i.e., finite element analysis) using ABAQUS (v6.14, ABAQUS Inc.). In this study, we tested two different prosthetic feet (see Fig. 1) that were created based on the previous studies [11], [12] by conducting a walking experiment. Both feet were made with onyx filament (i.e., short carbon fiber reinforced nylon filament with a diameter of 1.7 mm) using a desktop 3D printer (Mark Two, Markforged, Watertown, MA, USA). This enables the printed feet to provide more flexibility compared to acrylonitrile butadiene styrene (ABS) or polylactic acid (PLA). Build orientations were the same for both feet, and a printing layer height of 0.1 mm and a 100% fill density were set while printing them.

The foot in Fig. 1(a), named a flat-toe (FT) foot, was presented in [11]. This foot has re-entrant honeycomb structures with small curvatures (i.e., bending zones) at its forefoot. The FT foot achieved up to 15° toe flexion within the yield strength of the onyx [11]. Toe stiffness followed the human trend [19],

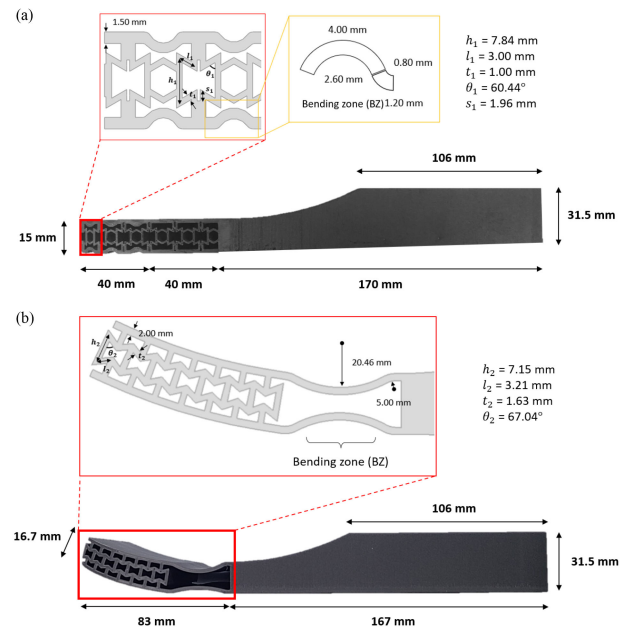


Fig. 1. 3D printed prosthetic feet using onyx filament. (a) FT foot with re-entrant honeycomb structure and bending zone. (b) CT foot with re-entrant structure and bending zone.

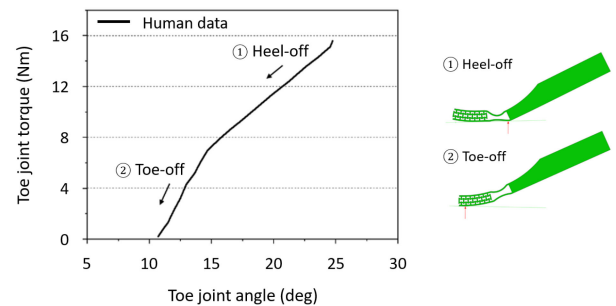


Fig. 2. Human toe joint angle-torque curve from heel-off to toe-off [19].

which has non-linearity from heel-off to toe-off (Fig. 2). However, 15° of toe flexion was not enough considering the human walking. To achieve a suitable bending structure of more than 20° , we recently proposed another prosthetic foot, designed using re-entrant structures (Fig. 1(b)) [12]. This curved-toe (CT) foot also has a bending zone at the forefoot to enhance the bending characteristics. This enables bending deformation to occur stably without causing unnecessary deformation at the curved part. All the dimensions of the structure and the foot were obtained by solving the optimization problem based on human data [20].

B. Powered Prosthetic System

1) *Hardware*: We used a custom-designed powered transfemoral prosthesis, AMPRO II, to investigate the effect of the prosthetic foot on walking biomechanics (Fig. 3). The prosthesis was operated by a microprocessor (BeagleBone Black, Texas Instruments, Dallas, TX, USA) to control the actuated ankle and knee joints. Force sensors (FlexiForce A502, Tekscan, South

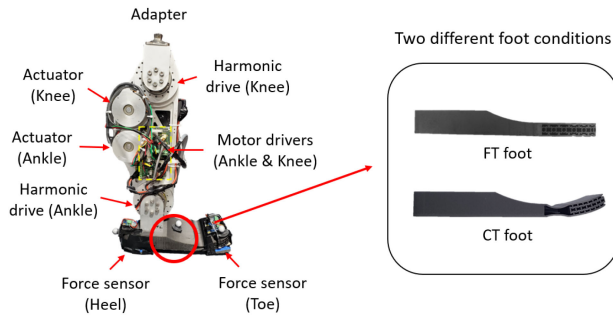


Fig. 3. AMPRO II: A custom-designed powered transfemoral prosthesis at Texas A&M University. Two different feet were given and compared.

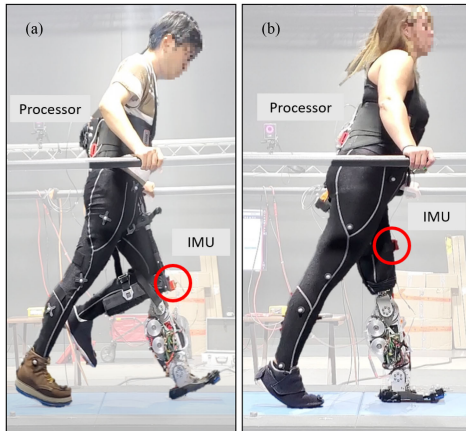


Fig. 4. (a) AB1 wears the prosthesis using the L-shape simulator. (b) TF1 wears the prosthesis with her own socket.

Boston, MA, USA) were placed under the heel and toe to detect important gait events, such as heel-strike, heel-off, and toe-off. The heel-strike was used as a cue for initiating the gait cycle and all the control parameters. An inertial measurement unit (IMU; MPU 9150, SparkFun Electronics, Niwot, CO, USA) was placed on the user's thigh to measure the thigh segment angle, which was then used to estimate the user's walking progression Fig. 4. The kinematics and kinetics of the prosthesis-side ankle and knee joint were collected using high-resolution optical encoders (E5, US Digital, Vancouver, WA, USA) and motor drivers (Gold-Solo Whistle, Elmo Motion Control, Petach-Tikva, Israel), respectively. The prosthetic foot was easily interchangeable to validate its effect on the gait performance of the prosthesis (Fig. 3).

2) *Phase Variable*: Estimating the user's walking state is important for prosthesis control because the prosthesis requires synchronized control with the user for stable walking. A phase variable (PV) is one method for estimating the user's walking state for the prosthesis control. [21], [22]. This variable indicates the user's walking state regardless of time by parameterizing the gait cycle based on kinematic changes in the user. To compute the PV in this study, we used thigh kinematics measured by an IMU attached to the thigh (Fig. 4). This is because the amputee's residual thigh moving in a periodic and consistent pattern during the gait cycle [21], [22]. As described in Appendix I, the resulting

TABLE I
SUBJECT INFORMATION: ABLE-BODIED AND AMPUTEE SUBJECTS

| Subject | Age | Gender | Weight (kg) | Height (m) | Amputation |
|---------|-----|--------|-------------|------------|--------------|
| AB1 | 32 | Male | 70 | 1.70 | N/A |
| AB2 | 27 | Female | 51 | 1.64 | N/A |
| TF1 | 23 | Female | 66 | 1.64 | Transfemoral |

PV (i.e., ϕ) was strictly monotonic and bounded in the range of $[0, 1]$, corresponding to 0%–100% of the gait cycle.

3) *Control Framework*: AMPRO II was controlled based on a hybrid control framework of impedance and proportional-derivative (PD) controllers [22], [23]. During the stance phase, the impedance controller provides a human-like joint torque for each joint based on the user's walking state as follows [23]:

$$\tau = K(\phi) \cdot (\theta_{act} - \theta_{eq}) + D(\phi) \cdot \dot{\theta}_{act}, \quad (1)$$

$K(\phi)$ and $D(\phi)$ refer to the stiffness and damping parameters that are functions of the PV for each joint, respectively. θ_{eq} denotes the equilibrium angle at different gait phases: 1) heel-strike to foot-drop, 2) foot-drop to heel-off, and 3) heel-off to toe-off [23]. Finally, θ_{act} and $\dot{\theta}_{act}$ are the instantaneous position and velocity of the joint as measured by the optical encoders. The impedance controller is highly responsive to the user's kinematics, allowing the user to interact with the ground more during the stance phase [24].

$$\tau = K_p \cdot (\theta_{act} - \theta_{des}(\phi)) + K_d \cdot (\dot{\theta}_{act} - \dot{\theta}_{des}(\phi)), \quad (2)$$

where $\theta_{des}(\phi)$ and $\dot{\theta}_{des}(\phi)$ denote the desired position and velocity of each joint, while θ_{act} and $\dot{\theta}_{act}$ denote the position and velocity for each joint. The proportional and derivative gains are denoted by K_p and K_d , respectively. As shown above, the PD controller was used to follow the desired joint trajectories during the swing phase. To generate the desired trajectories, third-order Bezier polynomials were used during the early swing phase for a smooth transition from the stance phase, and another set of third-order polynomials was used for foot clearance during the rest of the swing phase [22]. All the impedance parameters (i.e., stiffness and damping coefficients) and the desired trajectories were given based on PV (i.e., ϕ) to provide synchronized control with the user.

III. EXPERIMENTAL PROTOCOLS

A. Experiment Design

An indoor walking experiment was conducted with two able-bodied individuals (AB1 and AB2) and one unilateral transfemoral amputee (TF1), as summarized in Table I. The able-bodied subjects utilized an L-shape simulator to simulate the amputee walking with the prosthesis, and the amputee subject utilized her own socket, as depicted in Fig. 4. TF1 has been using an X3 Knee in conjunction with a Freedom Runway Foot (Otto-bock, Duderstadt, Germany). All walking trials were carried out on an instrumented treadmill (Tandem, AMTI, Watertown, MA, USA) while a 44 camera-based motion capture system (Vantage V5, Vicon, Hauppauge, NY, USA) collected the subjects' ground reaction forces (GRFs) and 3D motion data.

Prior to collecting the experimental data, the subjects underwent eight training sessions for two months for the subjects to get used to the powered prosthesis and the prosthetic feet. Each training session of 5–6 trials lasted for an hour. Subjects walked for 1–2 minutes each trial, and 10–15 minutes of break time was given between trials. For each trial, the prosthetic foot was randomly interchanged to avoid any bias from the foot.

During the validation session, data collection was performed for both feet (i.e., FT and CT feet) on the same day for each subject. Each trial lasted 90 seconds for walking and 15 minutes of break time were provided between each trial. To avoid fatigue and any potential safety issues, subjects walked at their preferred speed throughout all trials. With handrails on either side of the treadmill, safety was ensured. All the experiment protocol has been reviewed and approved by the Institutional Review Board (IRB) at Texas A&M University (IRB2015-0607F).

B. Data Analysis

We collected and interpolated the subject's motion capture data using Vicon Nexus. The marker data and GRFs were filtered with a third-order Butterworth low-pass filter based on a 10 Hz and 20 Hz cutoff frequencies, respectively. The associated lower-body model was constructed in Visual3D (C-Motion, Germantown, MD, USA). We collected the spatiotemporal metrics using the prosthesis sensors (e.g., encoders and force sensors), marker data, and force plate data. The prosthesis joint kinematics and kinetics were all calculated in the sagittal plane. The toe joint angle was also estimated in the sagittal plane using three markers on the prosthetic feet: heel, mid-foot, and toe. We estimated the toe joint angle by calculating the angle between the foot vector (i.e., heel to mid-foot) and the toe vector (i.e., mid-foot to toe). The timings of heel-off and toe-off were detected using the force sensors at the heel and toe.

To examine how much the foot condition affects symmetry between the prosthesis and the opposite side, we performed gait symmetry analysis. Gait symmetry is one of the outcomes in measuring gait patterns or evaluating gait performance [25]–[27]. Asymmetric gait is known to be inefficient in energy consumption during walking [28], [29] and may lead to asymmetric muscle activation on the low back [25], higher load on the intact limb and joints, and a higher risk of secondary impairments [30]. To evaluate the gait symmetry, we calculated the symmetry index (SI) based on both sides of the leg as follows [31]:

$$SI = \frac{(X_P - X_I)}{0.5 \cdot (X_P + X_I)} \cdot 100, \quad (3)$$

where X_P refers to prosthesis-side data and X_I refers to intact-side data. When the value of SI is equivalent to zero, it is referred to as a symmetric gait. On the other hand, when the value diverges from zero, referring to asymmetry. In this study, we investigated the symmetry of GRFs and stride time between bilateral legs. No statistical analyses were performed due to small sample size ($N = 3$) in this study.

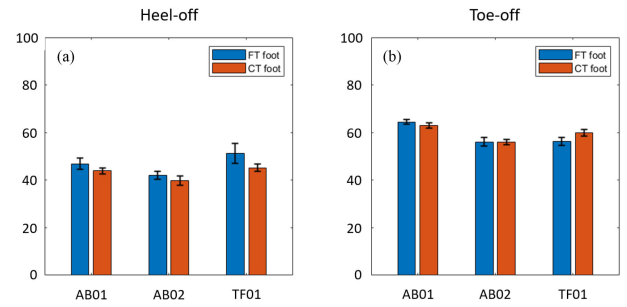


Fig. 5. Gait event detection in gait cycle (%): (a) Heel-off and (b) Toe-off. Blue indicates the FT foot, while red indicates the CT foot. Error bar indicates \pm one standard deviation (SD) of twenty gaits.

IV. RESULTS

A. Gait Event Detection

As shown in Fig. 5, the CT foot tended to have an earlier heel-off compared to the FT foot. In the case of toe-off, the AB subjects and TF1 showed different patterns. The AB subjects did not seem to have much difference in toe-off, whereas TF1 tended to have a later toe-off with the CT foot.

B. Prosthesis-Side Joint Kinematics/Kinetics

Fig. 6 shows the prosthesis-side ankle/knee joint kinematics and kinetics results of the amputee subject compared to healthy human data [32]. Both feet showed healthy human-like joint kinematics and kinetics trends while walking, but there was a discrepancy in timing for ankle push-off (e.g., Figs. 6(a) and (d)) and knee joint kinetics (e.g., Figs. 6(g) and (h)). This could be related to the difference between the healthy gaits and the amputee's gait. As shown in Fig. 6(c), the FT foot showed 4.5% greater ankle torque compared to the CT foot, resulting in greater plantar-flexion (Fig. 6(a)). Both the FT foot and the CT foot showed almost identical amounts of peak ankle joint power at approximately 50% of the gait cycle in Fig. 6(d). In the case of the knee joint, the CT foot showed 4% longer knee flexion during the stance phase and 2° more maximum flexion during the swing phase, as depicted in Figs. 6(e) and (f). There was no apparent difference between the two feet in knee joint kinetics, except the CT foot showed slightly longer knee flexion (Figs. 6(g) and (h)).

Fig. 7 shows the prosthesis-side ankle/knee joint kinematics and kinetics results of the able-bodied subjects. Compared to TF1, they both showed a later push-off, which is closer to human data [32] (Figs. 7(a) and (d)). There was no clear distinction between the two feet for AB1, but AB2 showed greater dorsiflexion, peak ankle torque, and peak ankle power with the CT foot in Figs. 7(a)–(d). The FT foot showed more maximum knee flexion and knee flexion at around 50% of the gait cycle than the CT foot (Fig. 7(e)). There was no apparent difference between the two feet in the other results of AB2 (see Figs. 7(f)–(h)).

Fig. 8 depicts TF1's mean trajectory of toe joint angle from 20 gaits. As depicted, TF1 had 5.72 times more maximum toe flexion with the CT foot than the FT foot (20.78° vs. 3.63°). Also,

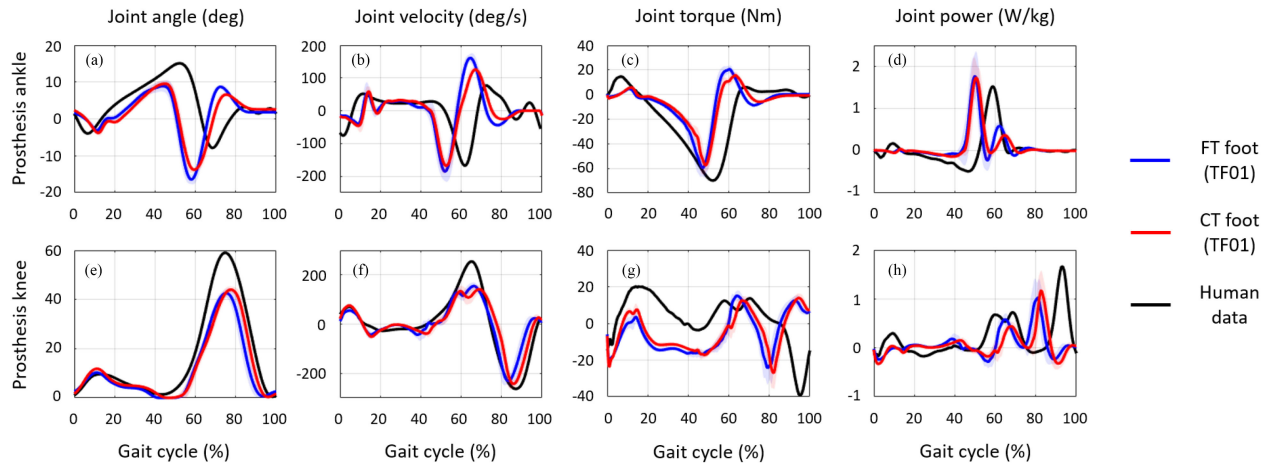


Fig. 6. Prosthesis-side joint kinematics/kinetics of TF1: (Top) Ankle, (Bottom) Knee. Results presented as mean \pm SD (shaded region) of 20 consecutive gaits. Blue indicates the FT foot, while red indicates the CT foot. Black indicates the human data from nine healthy subjects [32].

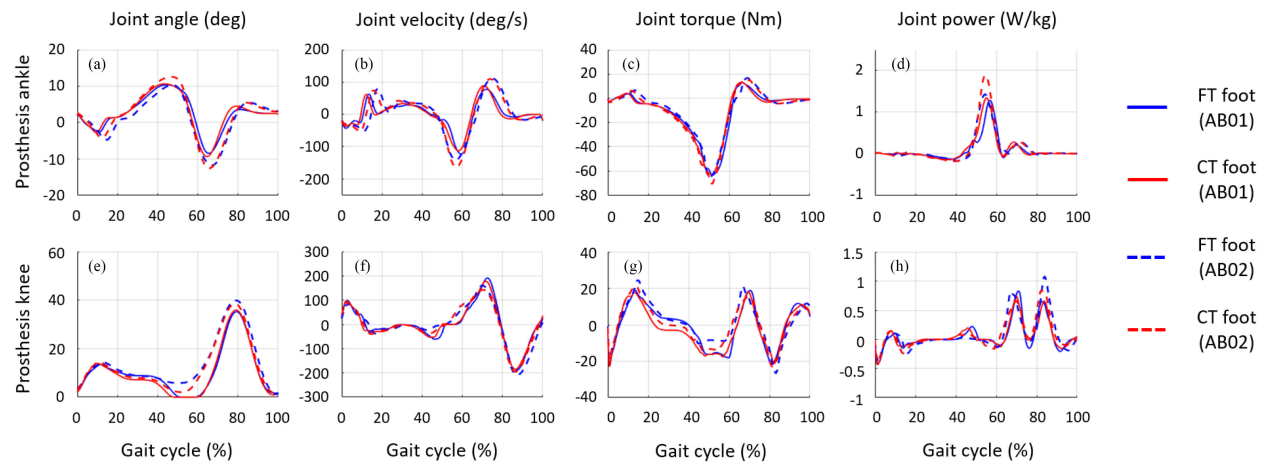


Fig. 7. Prosthesis-side joint kinematics/kinetics of AB1 (Solid) and AB2 (Dashed): (Top) Ankle, (Bottom) Knee. Blue indicates the FT foot, while red indicates the CT foot.

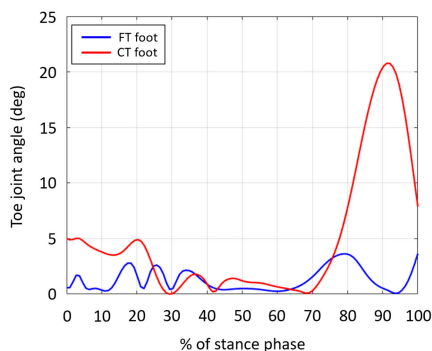


Fig. 8. TF1's mean trajectory of toe joint angle during the stance phase from 20 gaits. Blue indicates the FT foot, while red indicates the CT foot.

the maximum toe flexion occurred at about 90% of the stance phase with the CT foot, while it occurred at approximately 79% of the stance phase with the FT foot. In the case of healthy humans, they had the maximum toe flexion at about 50% of

the gait cycle, referring to approximately 83% of the stance phase [9]. This implies that the CT foot showed relatively late maximum toe flexion. This may be because the curvature of the CT foot is higher than that of humans.

Fig. 9 shows the push-off duration and the normalized push-off work during TF1's walking. Push-off is the phase that actually propels the human forward by providing a huge amount of positive work [33], [34]. As illustrated in Fig. 9(a), the push-off duration refers to how long this push-off phase lasts, and the normalized push-off work can be calculated by integrating the ankle power curve during this duration. Note that this phase lasted nearly 20% of the gait cycle in the case of healthy humans [33], [34], and the CT foot showed a longer push-off duration compared to the FT foot in Fig. 9(b) (FT foot: 10.59 ± 0.7760 vs. CT foot: 13.68 ± 0.8392 %). Interestingly, we could not find a distinct difference between the CT and FT foot's push-off work. However, it was clearly shown in Fig. 9(c) that the FT foot had about 2.7 times larger deviation in the push-off work compared to the CT foot.

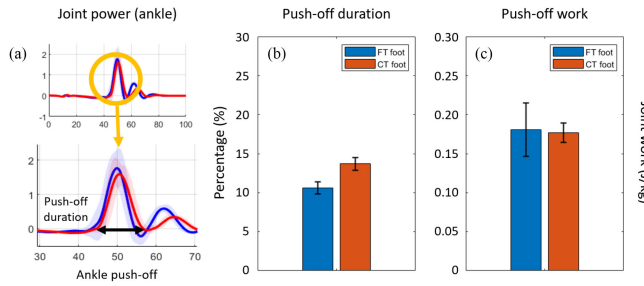


Fig. 9. Prosthesis-side (a) push-off duration and (b) normalized push-off work of TF1. Blue indicates the FT foot, while red indicates the CT foot. Bar indicates the mean of 20 gaits, and error bar is given with \pm SD.

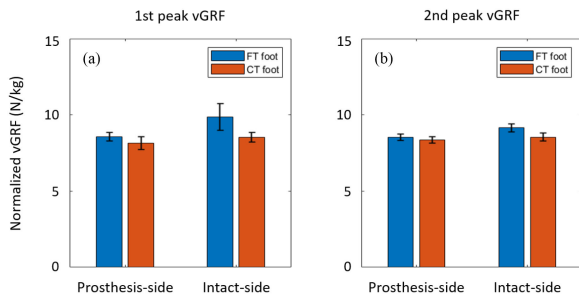


Fig. 10. GRF results of TF1: (a) 1st peak of vGRF, (b) 2nd peak of vGRF. Blue indicates the FT foot, while red indicates the CT foot. Bar indicates the mean of 20 gaits, and error bar is given with \pm SD.

C. Vertical Ground Reaction Force

Fig. 10 depicts the vertical ground reaction forces (vGRFs) of both the prosthesis-side and the intact-side legs of the subject. There are two peaks on the vGRF curve. The 1st peak of vGRF refers to the weight acceptance when the body weight is fully applied to the stance leg (Fig. 10(a)). The 2nd peak of vGRF refers to when the push-off occurs (Fig. 10(b)). Compared to the FT foot, the CT foot showed less vGRFs for both sides of the leg. More specifically, the prosthesis-side and the intact-side vGRF tend to decrease by 4.9% and 13.3%, respectively (Fig. 10(a)). The 2nd peak of vGRF showed a similar trend to the 1st peak of vGRF. With the CT foot, 2.1% and 6.7% reduced vGRFs were measured from the prosthesis-side and the intact-side, respectively.

D. Gait Symmetry

According to Fig. 10, the FT foot shows higher vGRFs from both the prosthesis and intact side legs. However, the vGRF differences between the prosthesis and intact sides were shown higher when the FT foot was utilized. Fig. 11 shows the gait symmetry using the symmetry index (SI) in (3). According to Fig. 11, the CT foot resulted in smaller SI for both the 1st peak vGRF and the 2nd peak vGRF compared to the FT foot. Fig. 11 also depicts the SI value using stride times. Note that the stride time refers to the duration of the gait cycle on the prosthesis side. There is no visible difference between the foot conditions, but the standard deviation of the FT foot's SI value is much greater than that of the CT foot.

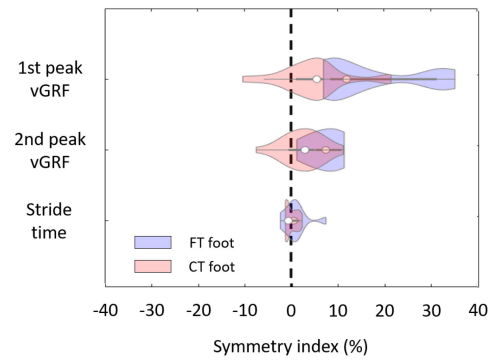


Fig. 11. Gait symmetry analysis: TF1. SIs of 1st peak of vGRF, 2nd peak of vGRF, and stride time are presented. Blue indicates the FT foot, while red indicates the CT foot. Error bar indicates \pm SD of 20 gaits.

TABLE II
RESULT SUMMARY OF TF1 (MEAN \pm SD OF 20 GAITS)

| | FT foot | CT foot |
|--------------------|---------------------|---------------------|
| Push-off duration | 10.590 \pm 0.7760 | 13.680 \pm 0.8392 |
| Push-off work | 0.1806 \pm 0.0341 | 0.1769 \pm 0.0125 |
| SI (1st peak vGRF) | 17.283 \pm 11.175 | 5.0106 \pm 7.5592 |
| SI (2nd peak vGRF) | 7.4348 \pm 3.6927 | 2.5831 \pm 4.1685 |
| SI (Stride time) | 1.7709 \pm 2.0415 | 1.1252 \pm 0.5436 |

V. DISCUSSION

We found that the CT foot tended to have an earlier heel-off and a later toe-off in Fig. 5. This could be interpreted that the curvature of the CT foot allowing the subject to have a more natural roll-over while walking, leading to a faster load transfer during the stance phase. This finding is well in line with the other studies [7], [8]; for instance, [8] reported that the center of pressure (COP) of the foot with 10° toe curvature passed through the toe joint center significantly earlier than the barefoot.

The push-off and SI results of TF1 are summarized in Table II. As shown in Fig. 9(a), the FT foot provided greater push-off power to the user than the CT foot. This trend can also be seen in other studies; the locked toe (i.e., without toe) showed greater average power during push-off than the flexible toe (i.e., with toe) [5], [10]. Having greater push-off may seem beneficial to the user; however, it may not be true. For instance, McDonald et al. reported a possible link between users' prosthetic foot preferences and which side of the leg they had an amputation on (i.e., dominant vs. non-dominant side) [5]. The amputee subjects who had the prosthesis on their non-dominant leg preferred the foot with less push-off power (e.g., the flexible toe), while the other subjects preferred the foot with greater power at the push-off (e.g., the locked toe). As shown in Fig. 9, the ankle motor consumed less average power during push-off with the CT foot but did the same amount of push-off work as the FT foot. This might be correlated with the collision loss from the intact leg (i.e., the leading leg). Collision loss is the negative work performed by the leading leg, which is known to be associated with step length: increased collision loss increases along with the increased step length [7], [35]. TF1 made a shorter step with the CT foot (0.4441 ± 0.0142 m) as opposed to the FT foot

TABLE III
MEAN \pm SD OF USER'S GAIT PHASE ESTIMATION RESULT

| | FT foot | CT foot |
|---------------------------|---------------------|---------------------|
| Linearity (R^2) | 0.9945 \pm 0.0042 | 0.9944 \pm 0.0022 |
| Linearity error (RMSE) | 0.0023 \pm 0.0005 | 0.0018 \pm 0.0004 |
| Heel-strike deviation (s) | 0.1306 \pm 0.0258 | 0.0872 \pm 0.0279 |

(0.4990 \pm 0.0308 m). Thus, we may be able to claim that the collision loss of the CT foot was less than that of the FT foot. This can also be found in Fig. 10; the CT foot showed a lower 1st peak vGRF than the FT foot, indicating that less impact occurred when the CT foot was used. When the FT foot was used, a greater collision loss in the intact side could have caused the following stance phase to be slower, causing the asymmetric gait [36]. This claim was supported by Table II that the FT foot provided a less symmetric gait to the user. Consistency of push-off work would be another interesting point. As shown in Fig. 9(b), the CT foot showed less than half amount of standard deviation in the push-off work than the FT foot. This could imply that the CT foot achieved more consistent push-off work than the FT foot. This consistency could also help the subject achieve better symmetry in the vGRFs while walking (Fig. 11).

According to Table III, interestingly, the CT foot also tended to affect the user's gait phase estimation (refer Section II.B.2). The linearity (R^2) refers to the coefficient of determination, which tells the linearity of the resulting PV while walking. The linearity error indicates the root-mean-square error (RMSE) between PV and the linear function during the gait cycle. The heel-strike deviation (i.e., heel-strike detection error) indicates the temporal difference between the actual heel-strike of the prosthesis and the estimated heel-strike of the user (i.e., when PV initially reaches 1). In other words, a smaller heel-strike detection error means that the gait phase estimator (i.e., PV) achieved a better estimation of the heel-strike. As found in Table III, error reductions in the linearity error and the heel-strike detection could be found when the CT foot was utilized. This may imply that the curvature of the foot affects the user's thigh kinematics, resulting in a better estimation of the user's gait phase.

There were some limitations in this study that can be addressed in the future to achieve a better gait using the toe-jointed foot. While the subject was walking using the FT foot or CT foot, she kept holding the handrails. Even though the subject went through the training sessions over two months to get used to it, she was less confident in walking using the prosthesis without holding the handrails because it was her first experience with the powered prosthesis. This may affect some of our results, such as GRFs. The harness will be a remedy to guarantee better safety while the subject is walking using the prosthesis in the future. Also, due to the limited time of training, we only collected the data at her preferred treadmill speed (i.e., 1.5 mph). Due to a lack of human models with toe joints, the toe joint kinematics was only presented in this study. Thus, more analysis regarding toe joints will be planned with a proper human model with toe

joints. Also, we plan to measure the energy consumption of the amputee subject while using the prosthesis. This will be another beneficial metric to evaluate the prosthesis and its foot in the amputee's ambulation. This study was based on a single amputee subject. A larger number of subjects is needed to investigate the effects of the proposed feet in general. We, therefore, plan to recruit more subjects for the follow-up study.

VI. CONCLUSION

In this study, we validated and compared two prosthetic feet that we proposed in our previous studies [11], [12]. We conducted a treadmill walking experiment with three subjects (i.e., two able-bodied and one amputee) using a custom-designed powered prosthesis. The foot condition (i.e., FT foot vs. CT foot) was altered during the experiment to compare two feet. As a result, the CT foot made a more natural roll-over possible during the stance phase, resulting in an earlier heel-off than the FT foot. This may be correlated to faster load transfer from the natural roll-over. This let the amputee subject have longer push-off duration with the CT foot, while the push-off work done with both feet showed no visible difference. With the FT foot, greater GRFs were found in both the prosthesis and intact sides when the heel-strike occurred (i.e., 1st peak of vGRF) and when the push-off occurred (i.e., 2nd peak of vGRF). On the other hand, the CT foot achieved better symmetry in both 1st and 2nd peak vGRFs than the FT foot. The curvature of the CT foot also affected the amputee's gait phase estimation, reducing the linearity error and improving the heel-strike detection. Future work will include the gait analysis, including toe joint kinetics and energy consumption, of more amputee subjects.

APPENDIX A

The PV can be computed based on the following assumptions: i) A thigh segment's angle profile $\theta(t)$ is a cosine-like function, and ii) The integral of the thigh segment's angle ($\Theta(t) = \int \theta(t) dt$) is a sine-like function. An ellipse represents the phase portrait of the thigh profile and its integral profile. Thus, a PV was calculated using the arc-tangent function, as below:

$$\phi(\Theta, \theta) = \frac{1}{2\pi} \text{atan2}(k(\Theta(t) - \alpha), (\theta(t) - \beta)), \quad (4)$$

where the scale coefficient k , the amplitude shift of the thigh integral α , and that of the thigh angle β , were defined by

$$k = \frac{|\theta_{\max} - \theta_{\min}|}{|\Theta_{\max} - \Theta_{\min}|}, \quad \alpha = \frac{|\Theta_{\max} + \Theta_{\min}|}{2}, \quad \beta = \frac{|\theta_{\max} + \theta_{\min}|}{2}. \quad (5)$$

To make $\phi(\Theta, \theta)$ bounded within [0,1], the final $\phi(\Theta, \theta)$ was computed as below:

$$\phi(\Theta, \theta) = \begin{cases} \phi(\Theta, \theta) & \Theta \geq \alpha \\ \phi(\Theta, \theta) + 1 & \Theta < \alpha \end{cases} \quad (6)$$

The normalizing factors (k , α , and β) made the phase portrait ($\theta(t)$ vs. $\dot{\theta}(t)$) center around the origin, reducing the PV's non-linearity. The integral value was initialized at every heel-strike, and the normalizing factors were updated every gait cycle to maintain the orbital radius during the gait cycle [22].

REFERENCES

- [1] J. Zhang, Y. Si, Y. Zhang, and Y. Liu, "The effects of restricting the flexion-extension motion of the first metatarsophalangeal joint on human walking gait," *Biomed. Mater. Eng.*, vol. 24, no. 6, pp. 2577–2584, 2014.
- [2] B. Jeong, S. Kim, J. Son, and Y. Kim, "Kinetic analysis of the metatarsophalangeal joint in normal subjects and hallux valgus patients during walking using a four-segment foot model," *J. Foot Ankle Res.*, vol. 7, no. 1, pp. 1–2, Apr. 2014.
- [3] F. Mager et al., "Determination of ankle and metatarsophalangeal stiffness during walking and jogging," *J. Appl. Biomech.*, vol. 34, no. 6, pp. 448–453, 2018.
- [4] E. C. Honert, G. Bastas, and K. E. Zelik, "Effect of toe joint stiffness and toe shape on walking biomechanics," *Bioinspiration Biomimetics*, vol. 13, no. 6, 2018, Art. no. 066007.
- [5] K. A. McDonald, R. H. Teater, J. P. Cruz, J. T. Kerr, G. Bastas, and K. E. Zelik, "Adding a toe joint to a prosthesis: Walking biomechanics, energetics, and preference of individuals with unilateral below-knee limb loss," *Sci. Rep.*, vol. 11, no. 1, pp. 1–10, 2021.
- [6] E. C. Honert, G. Bastas, and K. E. Zelik, "Effects of toe length, foot arch length and toe joint axis on walking biomechanics," *Hum. Movement Sci.*, vol. 70, 2020, Art. no. 102594.
- [7] P. G. Adamczyk, S. H. Collins, and A. D. Kuo, "The advantages of a rolling foot in human walking," *J. Exp. Biol.*, vol. 209, no. 20, pp. 3953–3963, 2006.
- [8] F. Sichtung, N. B. Holowka, O. B. Hansen, and D. E. Lieberman, "Effect of the upward curvature of toe springs on walking biomechanics in humans," *Sci. Rep.*, vol. 10, no. 1, pp. 1–11, 2020.
- [9] J. Zhu, Q. Wang, and L. Wang, "Effects of toe stiffness on ankle kinetics in a robotic transtibial prosthesis during level-ground walking," *Mechatronics*, vol. 24, no. 8, pp. 1254–1261, 2014.
- [10] L. Gabert, M. Tran, and T. Lenzi, "Design of an underactuated powered ankle and toe prosthesis," in *Proc. 43rd Annu. Int. Conf. IEEE Eng. Med. Biol. Soc.*, 2021, pp. 4920–4923.
- [11] H.-S. Kim, H.-J. Um, W. Hong, H.-S. Kim, and P. Hur, "3D-printable prosthetic foot with human toe-joint property," in *Proc. 44th Annu. Conf. Amer. Soc. Biomech.*, 2020, p. 546.
- [12] H.-J. Um, H.-S. Kim, W. Hong, H.-S. Kim, and P. Hur, "Design of 3D printable prosthetic foot to implement nonlinear stiffness behavior of human toe joint based on finite element analysis," *Sci. Rep.*, vol. 11, 2021, Art. no. 19780.
- [13] R. Gailey et al., "The effects of prosthesis mass on metabolic cost of ambulation in non-vascular trans-tibial amputees," *Prosthetics Orthotics Int.*, vol. 21, no. 1, pp. 9–16, 1997.
- [14] Y. S. Narang, V. M. Arelekatti, and A. G. Winter, "The effects of prosthesis inertial properties on prosthetic knee moment and hip energetics required to achieve able-bodied kinematics," *IEEE Trans. Neural Syst. Rehabil. Eng.*, vol. 24, no. 7, pp. 754–763, Jul. 2016.
- [15] T. Lenzi, M. Cempini, J. Newkirk, L. J. Hargrove, and T. A. Kuiken, "A lightweight robotic ankle prosthesis with non-backdrivable cam-based transmission," in *Proc. Int. Conf. Rehabil. Robot.*, 2017, pp. 1142–1147.
- [16] H. L. Bartlett, B. E. Lawson, and M. Goldfarb, "Design, control, and preliminary assessment of a multifunctional semipowered ankle prosthesis," *IEEE/ASME Trans. Mechatronics*, vol. 24, no. 4, pp. 1532–1540, Aug. 2019.
- [17] T. Li and L. Wang, "Bending behavior of sandwich composite structures with tunable 3D-printed core materials," *Composite Structures*, vol. 175, pp. 46–57, 2017.
- [18] T. Li, Y. Chen, X. Hu, Y. Li, and L. Wang, "Exploiting negative Poisson's ratio to design 3D-printed composites with enhanced mechanical properties," *Mater. Des.*, vol. 142, pp. 247–258, 2018.
- [19] E. M. Glanzner and P. G. Adamczyk, "Design and validation of a semi-active variable stiffness foot prosthesis," *IEEE Trans. Neural Syst. Rehabil. Eng.*, vol. 26, no. 12, pp. 2351–2359, Dec. 2018.
- [20] D. A. Winter, *Biomechanics and Motor Control of Human Movement*. Hoboken, NJ, USA: Wiley, 2009.
- [21] D. Quintero, D. J. Villarreal, D. J. Lambert, S. Kapp, and R. D. Gregg, "Continuous-phase control of a powered knee-ankle prosthesis: Amputee experiments across speeds and inclines," *IEEE Trans. Robot.*, vol. 34, no. 3, pp. 686–701, Jun. 2018.
- [22] W. Hong, N. Anil Kumar, and P. Hur, "A phase-shifting based human gait phase estimation for powered transfemoral prostheses," *IEEE Robot. Automat. Lett.*, vol. 6, no. 3, pp. 5113–5120, Jul. 2021.
- [23] N. Anil Kumar, S. Patrick, W. Hong, and P. Hur, "Control framework for sloped walking with a powered transfemoral prosthesis," *Front. Neuro-robot.*, vol. 15, 2022, Art. no. 790060.
- [24] B. E. Lawson, J. Mitchell, D. Truex, A. Shultz, E. Ledoux, and M. Goldfarb, "A robotic leg prosthesis: Design, control, and implementation," *IEEE Robot. Automat. Mag.*, vol. 21, no. 4, pp. 70–81, Dec. 2014.
- [25] C. Jayaraman et al., "Impact of powered knee-ankle prosthesis on low back muscle mechanics in transfemoral amputees: A case series," *Front. Neurosci.*, vol. 12, 2018, Art. no. 134.
- [26] S. Viteckova, P. Kutilek, Z. Svoboda, R. Krupicka, J. Kauler, and Z. Szabo, "Gait symmetry measures: A review of current and prospective methods," *Biomed. Signal Process. Control*, vol. 42, pp. 89–100, 2018.
- [27] E. Martini et al., "Increased symmetry of lower-limb amputees walking with concurrent bilateral vibrotactile feedback," *IEEE Trans. Neural Syst. Rehabil. Eng.*, vol. 29, pp. 74–84, 2020.
- [28] I. T. da Cunha-Filho, H. Henson, H. Qureshy, A. L. Williams, S. A. Holmes, and E. J. Protas, "Differential responses to measures of gait performance among healthy and neurologically impaired individuals," *Arch. Phys. Med. Rehabil.*, vol. 84, no. 12, pp. 1774–1779, 2003.
- [29] K. K. Patterson et al., "Gait asymmetry in community-ambulating stroke survivors," *Arch. Phys. Med. Rehabil.*, vol. 89, no. 2, pp. 304–310, 2008.
- [30] J. A. Block and N. Shakoob, "Lower limb osteoarthritis: Biomechanical alterations and implications for therapy," *Curr. Opin. Rheumatol.*, vol. 22, no. 5, pp. 544–550, 2010.
- [31] R. O. Robinson, W. Herzog, and B. M. Nigg, "Use of force platform variables to quantify the effects of chiropractic manipulation on gait symmetry," *J. Manipulative Physiol. Therapeutics*, vol. 10, no. 4, pp. 172–176, Aug. 1987.
- [32] K. R. Embry, D. J. Villarreal, R. L. Macaluso, and R. D. Gregg, "Modeling the kinematics of human locomotion over continuously varying speeds and inclines," *IEEE Trans. Neural Syst. Rehabil. Eng.*, vol. 26, no. 12, pp. 2342–2350, Dec. 2018.
- [33] K. E. Zelik and A. D. Kuo, "Human walking isn't all hard work: Evidence of soft tissue contributions to energy dissipation and return," *J. Exp. Biol.*, vol. 213, no. 24, pp. 4257–4264, 2010.
- [34] K. E. Zelik, K. Z. Takahashi, and G. S. Sawicki, "Six degree-of-freedom analysis of hip, knee, ankle and foot provides updated understanding of biomechanical work during human walking," *J. Exp. Biol.*, vol. 218, no. 6, pp. 876–886, 2015.
- [35] J. M. Donelan, R. Kram, and A. D. Kuo, "Mechanical work for step-to-step transitions is a major determinant of the metabolic cost of human walking," *J. Exp. Biol.*, vol. 205, no. 23, pp. 3717–3727, 2002.
- [36] P. G. Adamczyk and A. D. Kuo, "Mechanisms of gait asymmetry due to push-off deficiency in unilateral amputees," *IEEE Trans. Neural Syst. Rehabil. Eng.*, vol. 23, no. 5, pp. 776–785, Sep. 2015.